Carbohydrate Polymers 196 (2018) 376–384

Contents lists available at ScienceDirect

Carbohydrate Polymers

journal homepage: www.elsevier.com/locate/carbpol

Shape memory aerogels from nanocellulose and polyethyleneimine as a novel adsorbent for removal of Cu(II) and Pb(II)

Jian Li[a], Keman Zuo[a], Weibing Wu[a,*], Zhaoyang Xu[b], Yonggang Yi[a], Yi Jing[a], Hongqi Dai[a], Guigan Fang[c]

[a] Jiangsu Co-Innovation Center for Efficient Processing and Utilization of Forest Resources, Nanjing Forestry University, 159 Long pan Road, Nanjing 210037, China
[b] College of Materials Science and Engineering, Nanjing Forestry University, 159 Long pan Road, Nanjing 210037, China
[c] Institute of Chemical Industry of Forestry Products, Chinese Academy of Forestry, Nanjing 210042, China

ARTICLE INFO

Keywords:
Aerogel
Electrostatic combination
Shape memory
Heavy metal
Adsorbent

ABSTRACT

This study describes the preparation of an aerogel adsorbent based on nanofibrillated cellulose(NFC) and polyethyleneimine(PEI) via electrostatic combination without chemical crosslinking. Purely physical crosslinking between NFC and PEI was confirmed by attenuated total refraction-Fourier transform infrared spectroscopy (ATR-FTIR) and thermogravimetric analysis (TGA). The NFC/PEI hybrid aerogels exhibited good structural stability and shape recovery in water. Absorption experiment shows that the hybrid aerogels are excellent adsorbents for the removal of heavy metal ions owing to the highly porous structure and the existence of plenty of amine groups. Thermodynamic and kinetic study showed pseudo-second-order equation and Langmuir model ($R^2 > 0.999$) as the best fit. The maximum adsorption capacity of Cu(II) and Pb(II) according to Langmuir model was 175.44 mg/g and 357.44 mg/g, respectively. Besides, the Cu(II) or Pb(II) loaded NFC/PEI aerogel could be easily regenerated by EDTA and retain the adsorption capacity after repeatedly using. This environmentally friendly hybrid aerogels with high-performance are promising candidates for sewage disposal and metal pollution treatment.

1. Introduction

With the population expansion and the industrialization, heavy metals have become some of the most dangerous and extensive water pollutants, which is a serious problem for human society today. Among all, bivalent lead(Pb(II)) and copper(Cu(II)) are the most important because of their widely usage in industry such as electroplating, electrolysis, pesticides, photography, paper manufacturing and others (Khodadadi, Malekpour, & Ansaritabar, 2017; Mishra & Patel, 2009; Wang & Chen, 2006). For example, lead can lead to polymeric, lesions and even multiple organ failure in human beings even in extremely low concentration. High levels of copper can cause toxic effects like all other heavy metals. Thus, removing heavy metal ions from water is urgent and a high priority not only for the safety of water resources but ultimately for the survival of human beings. At present, many treatment methods have been applied to remove heavy metal ions from wastewater including, chemical reduction and precipitation, ion exchange, coagulation, flocculation, membrane filtration and adsorption (Barrera-Díaz, Lugo-Lugo, & Bilyeu, 2012; Owlad, Aroua, Daud, & Baroutian, 2009). Among the different approaches, adsorption is recognized as the most efficient approach regarding an easy implementation and a low operational cost (O'Connell, Birkinshaw, & O'Dwyer, 2008).

Aerogels are highly porous and network materials, having a number of excellent physicochemical properties such as high porosity, low density, high surface area and adjustable surface chemistry. It has drawn significant attentions as an adsorption media for removal of heavy metal ions (Carta, Casula, & Corrias, 2009; Ge, Yang, & Li, 2009; Zheng, Cai, & Gong, 2014). However, the adsorption capacities of common aerogels are quite low, probably due to the lack of surface affinity groups or lack of chemical adsorption, and there is no possibility of regeneration process on the adsorbent (Adebajo, Frost, & Kloprogge, 2003). Therefore, it is very necessary to explore aerogel materials for an easy, sustainable and highly efficient capture of heavy metal ions from the water sources.

Naturally derived nanocellulose including nanocrystal cellulose (NCC) and nanofibrillated cellulose (NFC) are emerging nanomaterials that display high surface area, high strength, and tunable surface chemistry, allowing for controlled interactions with polymers, small molecules, nanoparticles, and biological materials (Isogai, 2013). They are very suitable for creating reinforced or structured hydrogel or

* Corresponding author.
E-mail address: wbwu@njfu.edu.cn (W. Wu).

https://doi.org/10.1016/j.carbpol.2018.05.015
Received 9 February 2018; Received in revised form 16 April 2018; Accepted 4 May 2018
Available online 17 May 2018

aerogel composites exhibiting both mechanical reinforcement and a host of other desirable properties. Nanocellulose aerogels have high surface areas (10–284 m^2/g) and high porosity, and the surface carrying a large number of active functional groups such as hydroxyl, aldehyde, carboxyl compared to those common aerogels (Chen, Li, & Wang, 2014; Heath & Thielemans, 2010). However, there are still limitations for the application of pure nanocellulose aerogel as adsorbent. First, the pure nanocellulose aerogels were easily disintegrated in water (Lu, Hsieh, & You, 2012; Zhang, Zhang, & Lu, 2012). Extra chemical crosslinking (Chen, 2011; Heath & Thielemans, 2010) is usually required to improve wet strength. Second, the adsorption capacity of metal ions for pure nanocellulose is relatively low. Chemical modifications to introduce functional groups are mostly complicated and not environmentally friendly.

To solve above problems, we designed an aerogel adsorbent with wet strength based on cellulose nanofibrils (NFC) and polyethyleneimine (PEI). PEI is a widely used wet end agent to endure paper with wet strength in paper making. Besides, PEI has plenty of primary, secondary and tertiary amines on the macromolecular chains, which are effective functional groups to improve the adsorption capacity. The preparation of NFC/PEI aerogel is a purely physical procedure without any chemical treatment. Physically-crosslinked network of NFC and PEI was obtained via electrostatic combination. The NFC/PEI composite aerogels were used as absorbent for the removal of Pb(II) and Cu(II) from aqueous solution. The effects of pH, contact time, initial metal ion concentration, and temperature on the absorption, desorption and reusability were tested in batch experiments. The absorption, desorption performance and reusability of NFC/PEI aerogels were also investigated.

2. Materials and methods

2.1. Materials

Softwood pulp (Asia Pacific Senbo (Shandong) Pulp & Paper Co., Ltd., China) was used as an original material for preparing NFC. Ethylene inine polymer (PEI) (70,000, 50% solution in water) was obtained from Aladdin industrial corporation (Shanghai, China), 2,2,6,6-Tetramethylpiperidine 1-oxyl (TEMPO, Sigma Aodeliqi, US A), hydrochloric acid, nitric acid, sodium hydroxide, sodium hypochlorite, sodium bromide, ethylenediaminetetraacetic acid (EDTA), $CuSO_4{\cdot}5H_2O$, and $Pb(NO_3)_2$ (Nanjing Chemical Reagent Co., Ltd, China) were all of laboratory grade and used without further 3 purification.

2.2. Preparation of nanofibrillated cellulose (NFC)

NFC was prepared via TEMPO/NaClO/NaBr oxidation system (Benhamou, Dufresne, Magnin, & Mortha, 2014). Never-dried bleached softwood pulp (10 g) was suspended in deionized water (500 mL) containing TEMPO (0.16 g) and NaBr (1.6 g). An aliquot of 7.6 mmol/L NaClO solution (120 mL) was added to the cellulose slurry, and the pH was maintained at 10.5 by adding 0.2 mol/L NaOH at room temperature under mechanical agitation. The reaction was stopped when no more decrease in pH was observed (Fukuzumi, Saito, & Isogai, 2013). The resultant samples were purified using 0.1 mol/L HCl solution and finally ultrasonicated at consistency of 1 wt% for 5 min at 300 W to obtain the NFC solution.

2.3. Preparation of NFC/PEI composite hydrogels (NPHxy) and aerogel (NPAxy)

Cylindrical HDPE (high density polyethylene) cups (40 mm in diameter, 50 mm in height) were used as molds for the preparation of the aerogels. Firstly, the NFC aqueous solution (1 wt%, pH 10) was sonicated for 15 min, and the PEI solution was diluted from 50% to 25% by using deionized water to adjust the pH to 10. Then the NFC was mixed with PEI solution and the mixture was diluted to the total volume of 20 mLwith deionized water. The weight ratios of NFC and PEI were designed differently but the total concentration of NFC and PEI was kept at 12 mg/mL. The suspension was homogenized under magnetic stirring and stood at room temperature for 4 h to get hydrogel. Aerogels were obtained by freeze-drying for 3 days at −91 °C with a freeze-dryer after pre-freezing the sample at −20 °C for 12 h. The resulted hydrogel and aerogel were named as NPHxy and NPAxy respectively, where x and y are the weight ratios of NFC and PEI. Here, the weight ratios of 1:3, 2:2 and 3:1for composite aerogels are referred as NPA13, NPA22 and NPA31, respectively. The concentrations of pure NFC and PEI suspensions were also controlled at 12 mg/cm^3.

2.4. Characterization

The NPAs were determined by scanning electron microscopy (SEM, JEOL JSM-7600F, Japan). Attenuated total refraction Fourier-transform infrared spectroscopy (ATR-FTIR) were recorded using a FTIR-650 spectrometer (Tianjin Gangdong Science and Technology Co, Ltd., China) with the wavenumber range of 4000–400 cm^{-1}. Thermogravimetric analysis (HTG-3, Beijing long Technology Co, Ltd., China) was performed from 25 °C to 600 °C with a heating rate of 10 °C/min under nitrogen atmosphere. The surface zeta potentials of the NPAs were obtained using a zeta potential analyzer (NanoPlus-2, Micromeritics Co, Ltd., China). The BET specific surface area and pore size distribution of NPAs were measured by N_2 adsorption/desorption at −196 °C using a Quantachrome FVD-3 surface area analyzer.

2.5. Adsorption studies

Adsorption experiments were conducted by the batch method to examine the sorption kinetics and sorption isotherm of Cu(II) and Pb(II) ions by NPAs. NPAs adsorbents (60 mg) and metal ion solution (200 mL) were added into a 250 mL flask. Then the flask was placed in a water bath shaker at 150 rpm to reach the adsorption equilibrium. The adsorption temperature was kept at 25 °C. The sorption isotherm experiments were conducted under different metal ion concentrations ranging from 20 mg/L to 200 mg/L. The metal ion concentration at equilibrium was determined by the atomic absorption spectrophotometer SK-2002B (Beijing Hua Yang Analytical Instrument Co, Ltd., China) and the equilibrium adsorption capacity (q_e, mg/g) was analyzed according to Eq. (1):

$$q_e = \frac{(C_0 - C_e)*V}{m} \tag{1}$$

where C_0 and C_e (mg/L) are the initial and equilibrium metal ion concentrations in the aqueous solution; V (mL) is the volume of the solution and m (mg) is the adsorbent dose.

2.6. Data analysis

The adsorption kinetic data of the Cu(II) and Pb(II) onto NPAs were simulated with the pseudo-first- and second-order kinetic models, which were expressed as Eqs. (2) and (3):

$$\log(q_e - q_t) = \log q_e - \frac{k_1 t}{2.303} \tag{2}$$

$$\frac{t}{q_t} = \frac{1}{k_2 q_e^2} + \left(\frac{1}{q_e}\right) t \tag{3}$$

Where q_e and q_t (mg/g) are adsorption capacities at equilibrium and time t, k_1 (min^{-1}) and k_2 (g/(mg min)) are rate constants of pseudo-first and second-order adsorption, respectively.

The adsorption isotherms of Cu(II) and Pb(II) adsorption by NPAs. The Langmuir and Freundlich adsorption isotherm models were employed to analyze the experimental data, which were represented as

Eqs. (4) and (5):

$$\frac{C_e}{Q_e} = \frac{C_e}{Q_m} + \frac{1}{Q_m b} \quad (4)$$

$$lgQ_e = lgk_f + \frac{1}{n} lgC_e \quad (5)$$

where Q_e (mg/g) is the equilibrium adsorption capacity, C_e (mg/L) is the metal ion solution concentration at equilibrium, Q_m (mg/g) is the maximum adsorption capacity and b is the Langmuir adsorption constant related to adsorption energy, K_f and n are the Freundlich adsorption constants which indicate the capacity and intensity of the adsorption, respectively.

3. Result and discussion

3.1. Synthesis and characterization of NPAs

Chemical or physical crosslinking is generally required to fabricate hydrogels and further aerogels with three-dimensional network (Liang et al., 2012) Chemical crosslinking methods including monomer polymerization, covalent linking, and graft copolymerization usually possess the problems of using toxic reagents and chemical residue (Hüsing & Schubert, 1998). Physical crosslinking via electrostatic interaction, hydrogen bonding, hydrophobic association or chain winding can avoid above problems (Cong, 2012). In addition, the technology of physical crosslinking is much simpler. In this work, we tried to prepare NFC based hydrogels and aerogels via electrostatic interaction considering that there are a large number of negative carboxyl groups on the surface of NFC. It has been reported that alginate is a polysaccharide that can be cross-linked with two valent cations (Ca^{2+}, Sr^{2+}, Ba^{2+} and other cations) to form hydrogel with uniform network structure (Zander & Nicole, 2014). However, this method was not suitable to prepare NFC based hydrogel here. Flocculation rather than gel quickly formed when calcium ion was added to NFC solution. Reason may be that the charge neutralization effect of calcium compress the electric double layer of NFC and cause the aggregation of NFC (Dong, 2013). Due to the mobility of NFC in aqueous solution and the high electrostatic interaction between NFC and calcium, the aggregations of NFC were relatively compact, leading to inhomogeneous flocculation rather than uniform gel. In order to obtain a uniformly crosslinked network, we tried another aggregation method of bridging interaction in replace of charge neutralization using cationic electrolyte with high molecular weight. Here, PEI, a widely used cationic wet end agent with molecular weight of 70 000, was selected. First, the mixing of NFC and PEI was conducted at neutral condition, no gel but flocculation quickly formed before a uniform mixture of NFC and PEI was obtained. We believe that the intensity of electrostatic interaction between NFC and PEI plays a critical role during the formation of hydrogel. As shown in Fig. 1a, the Zeta potentials of NFC and PEI are −10.54 and 16.25 mV at pH of 7, respectively. Obviously, strong electrostatic interaction between NFC and PEI would occur at these high values, leading to intense aggregation between NFC and PEI and further inhomogeneous flocculation (See Supporting information, Fig. S1). The change rule of Zeta potentials shows that it is possible to tune the electrostatic interaction between NFC and PEI by changing the pH value. From pH 7 to pH 10, the Zeta potential of NFC increases from −10.54 to −36.14 mV, but the Zeta potential of PEI decreased from 16.25 to 3.89 mV. The Zeta potential of NFC and PEI mixture is negative and is comparable to that of pure NFC at pH 10. Although there is no specific data about the electrostatic interaction, the slow gel procedure with gradually increased viscosity (Fig. 2b) indirectly indicated the electrostatic interaction between NFC and PEI was appropriate. The gel procedures of hydrogels generally finished in the period of 1–4 h (Fig. 1c). The hydrogel from 10 mg/mL NFC or 25 mg/mL PEI solution alone cannot be formed. The mixture viscosity increased and the required time for gel was reduced when there was an increase in the ratio of NFC and PEI. In order to investigate the effect of hydrogen bonding interaction on gel formation, mixture of NFC and PVA was prepared for comparison (See Supporting information, Fig. S2). However, it was found that pure hydrogen bonding interaction between NFC and PVA could not trigger the gel formation. In addition, high molecular weight of PEI was also important for the hydrogel formation. Aerogels from the hydrogels of NFC and PEI with low molecular weight was found of extremely low mechanical strength. Scheme 1 depicts the synthesis of NPH and NPA with physically-crosslinked three-dimensional network via electrostatic combination. Here, PEI with high molecular weight and branched structure was selected and alkaline condition was applied to realize a controllable gel procedure of NFC. Above all, moderate electrostatic combination and a slow gel procedure were required to produce uniform and stable network hydrogel via electrostatic combination.

The FTIR spectra of PEI, NFC, NPAs are presents in Fig. 2a. The characteristic peaks observed for NFC spectra at 3334 cm^{-1}, 2941 cm^{-1} and 1723 cm^{-1} are related to O—H stretching, asymmetric C—H stretching and carboxyl stretching, respectively (Salama, Shukry, & El-Sakhawy, 2015). For PEI, the absorption at 2842 cm^{-1}, 1556 cm^{-1}, and 1168 cm^{-1} were the characteristic peaks of $-CH_2-$ stretching vibrations, amino group and C—C skeleton vibration, respectively (Zhang, Zang, & Shi, 2016). All of the above characteristic peaks appeared in the NPAs and no new peaks generated. The result of FTIR spectra proved that the NPAs were physical blends and no chemical crosslinking occurred.

Fig. 2b shows the thermogravimetry curves of NFC, PEI and NPAs. Generally, NPAs combines the thermogravimetry characteristics of NFC and PEI. The NPAs weight losses occurred at two different temperature ranges. The first stage of weight loss ranging from 200 to 300 °C, might be attributed to the cellulose degradation (Nair, Zhu, & Deng, 2014). The second stage of weight loss beginning at around 300 °C and completing at about 400 °C, might be attributed to the fracture of the PEI chain (Hong & Joo, 2009). However, it is noted that the initial decomposition temperatures of NPAs are lower than those of NFC and PEI. The contribution to the reduced NPAs thermal stability may come from the electrostatic interaction between ionized NFC and PEI.

3.2. Shape recovery of NPAs

NPAs were obtained via freeze drying of NPHs. Structural contraction and collapse were observed for NPA13, whereas NPA22 and NPA31 maintained the outline structure well after freeze drying. SEM measurements were conducted to investigate the inside structure of NPAs. As shown in Fig. 3, NPA13 shows lots of closed pores and fiber film structure, which also reflect the structural contraction and collapses. NPA22 and NPA31 possess open and macroporous honeycomb structure. As the NFC content increases, the homogeneity of microporous structure is gradually improved and the BET specific surface area increases from 15.2 m^2/g of NPA13 to 42.5 m^2/g of NPA31 (Fig. S3), indicating that NFC plays a critical role in constructing the skeleton frame of aerogels and preserving integrity during the drying process. With interconnected macroporous structure and physical integrity, NPAs showed superior capability of water absorption and good performance of shape recovery (Movie S1). Details of NPA22 are shown in Fig. 4. When immersed in water, compressed NPA-2 rapidly absorbed water at around 50 times its own weight and returned to its original state without noticeable changes in the volume or shape. None of the aerogels showed noticeable expansion upon absorption and the absorbed water could be easily squeezed out, indicating that the absorbed water mainly filled in the open pores. The shape recovery ability of the NPAs may be caused by the interaction between the absorbed water and NFC. The elastic modulus of the crystal region of cellulose ranges from 130 to 250 GPa (Sakurada, Nukushina, & Ito, 1962; Zimmermann, Bordeanu, & Strub, 2010), while that of the amorphous region is reported to be 12.2 or 10.4 GPa (Chen, Lickfield, & Yang, 2004; Wang,

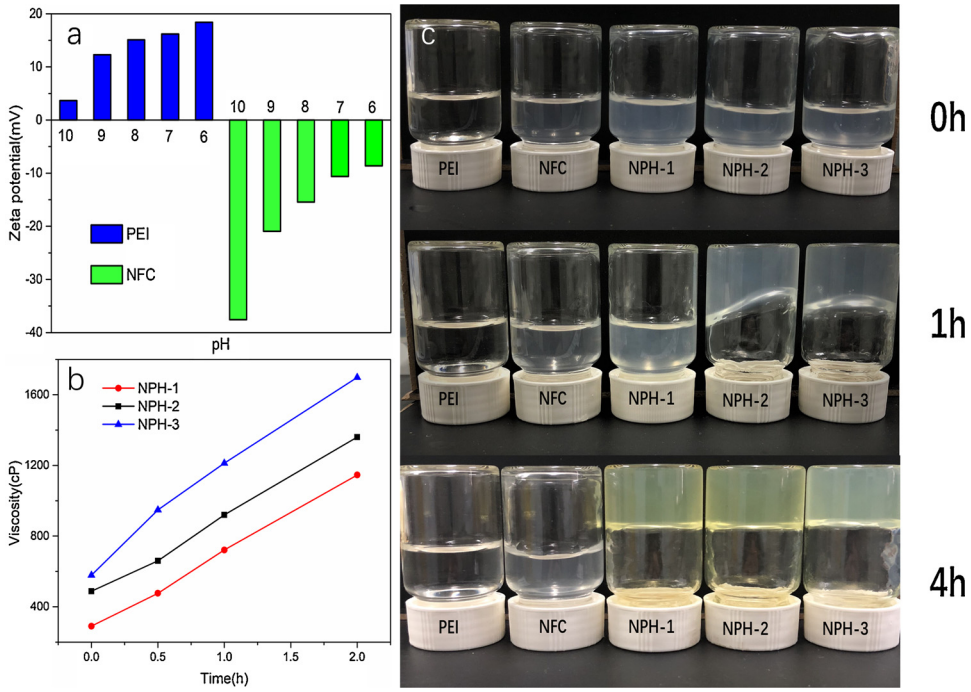

Fig. 1. (a) Zeta potentials of NFC, PEI at different pH values; (b) Sol suspension viscosities of NFC (pH 10) and PEI (pH 10) mixtures with increasing time,; (c) Digital pictures of the formation of NPHs from 0 to 4 h.

Tian, & Xu, 2014). Due to this substantial difference in the elastic moduli in the crystalline and amorphous regions of cellulose, the bending of NFC under compression is confined to the amorphous region. When the compressed NPAs absorb water, the amorphous region swells partially, causing the NFC to expand to a more stretched form and recovers its original shape. It was noteworthy that pure NFC aerogels without PEI did not show shape recovery. Pure NFC aerogels gradually disintegrated when immerged in water. It indicates that the capability of PEI to enhance wet strength is also important for the performance of shape recovery besides the characteristic of NFC. Due to the existence of plenty of amine groups and the detected positive Zeta potential of PEI, a large number of ionic bonds between the protonated amine and carboxyl and hydrogen bonds between amine and hydroxyl can form (Sui, Cui, Zhu, & Han, 2013). This new combination between NFC and PEI which will not be destroyed in a short period of time, guaranteeing the structural integrity of 3D network NPAs.

Over 90% of absorbed water could be easily removed by hand squeezing the NPAs into a compact round plate. The compressed NPA22 could reabsorb water instantaneously and return to the original size and shape in 1.9 s, showing excellent water-activated shape recovery. The NPA22 was found withstanding hand squeezing without breaking or falling apart even after over 80 cycles, exhibiting excellent wet strength and reusability. The performance of NPAs is similar to that of wet strength paper, in which PEI enhances and protects the network structure of fibers. NPAs with low content of PEI, for instance, NPA31, has lower wet strength and fewer cycle times compared to NPA22. It is reasonable since there is no resistance for the hydrogen bonding combination between NFC to water in spite of its uniform porous structure.

3.3. Adsorption kinetics

Taking into account of the morphology, porous structure, shape recovery and functional groups of NPAs, NPA22 was selected to as ideal adsorbent to investigate the adsorption properties. The adsorption rate

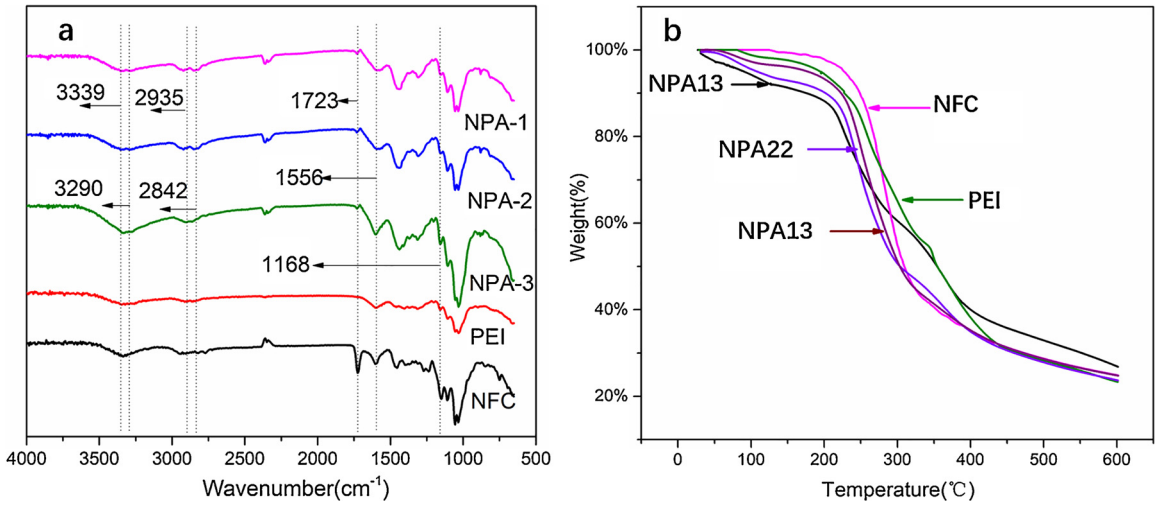

Fig. 2. (a) FTIR spectra of NFC, PEI and NPAs (b) TGA curves of NFC, PEI and NPAs.

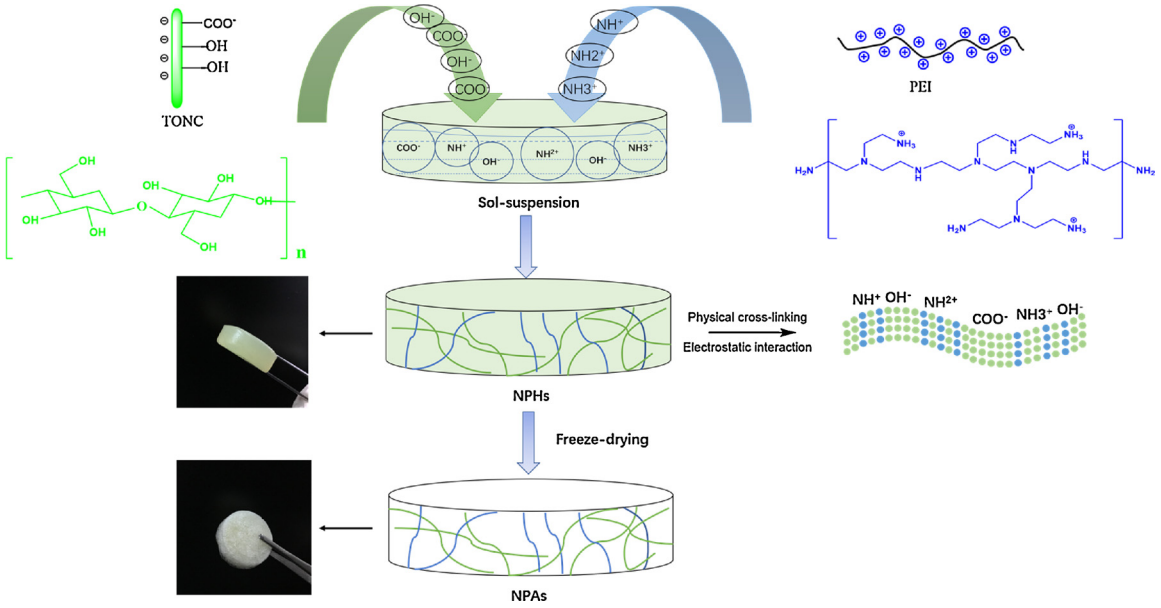

Scheme 1. Synthesis route of NPHs and NPAs.

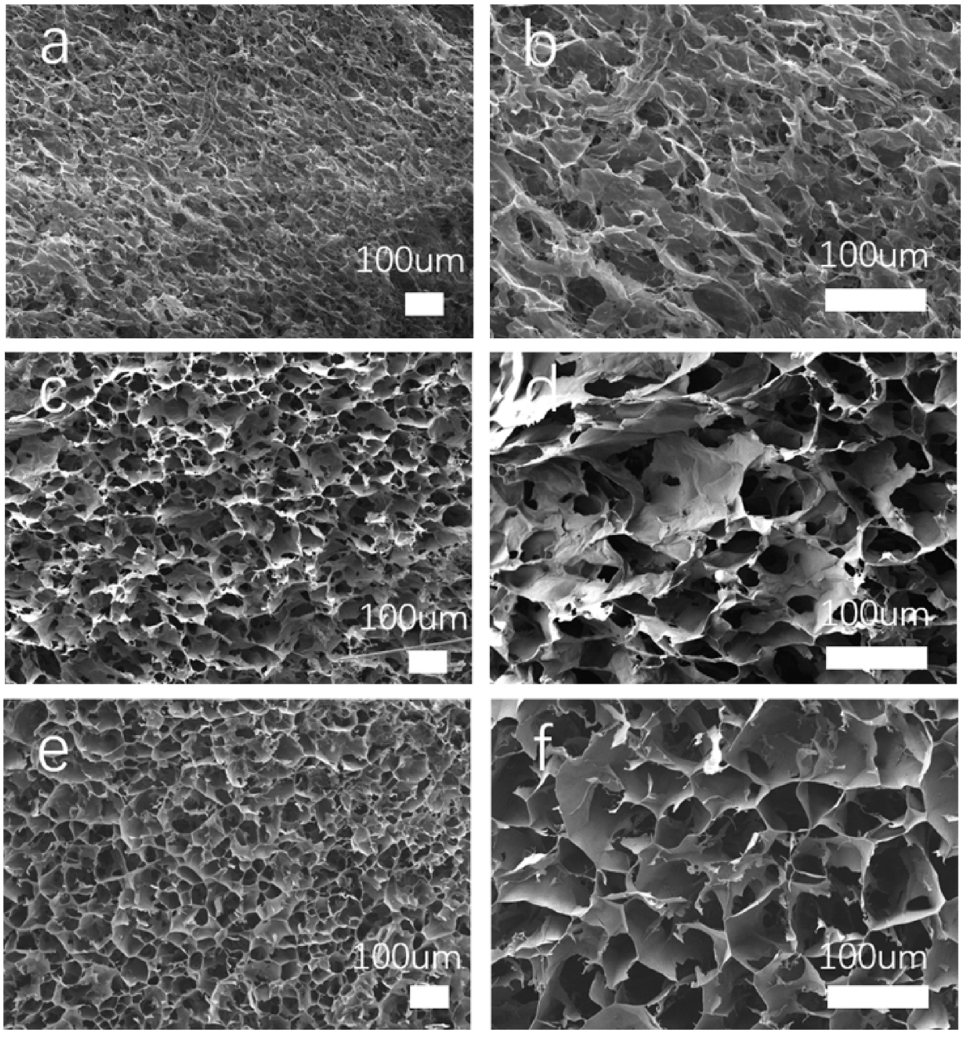

Fig. 3. SEM images of NPAs (a, b: NPA13; c, d: NPA22; e, f: NPA31).

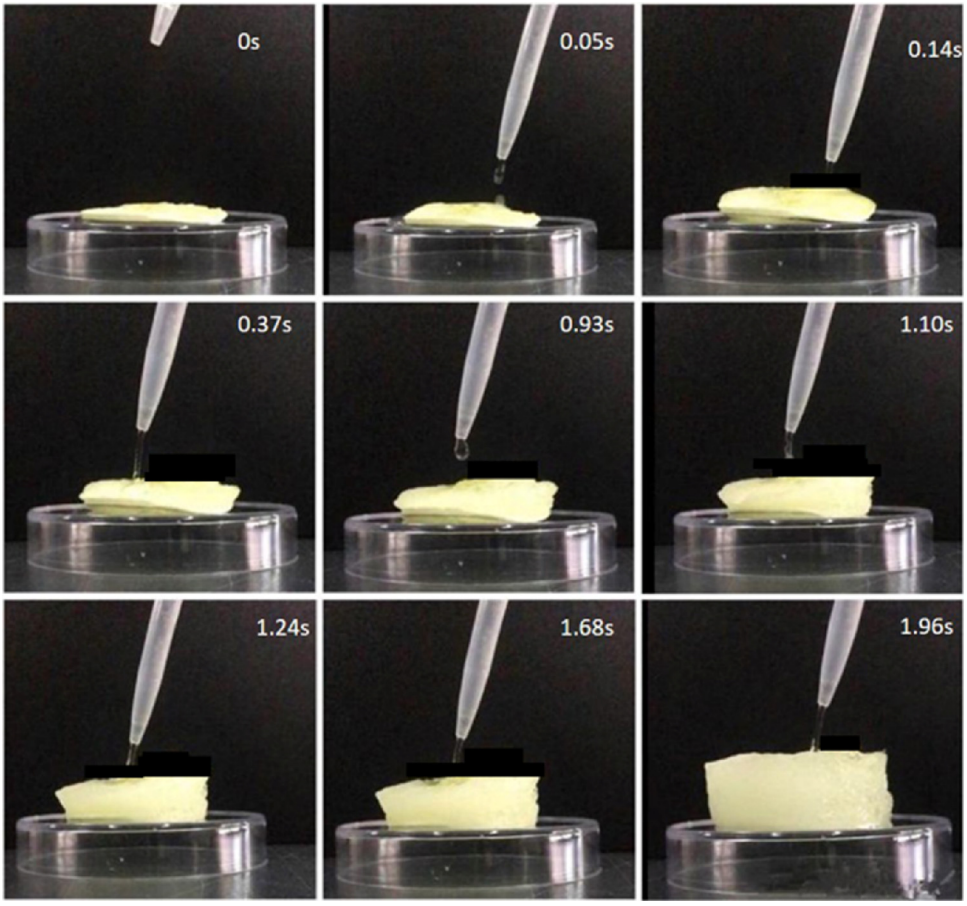

Fig. 4. Shape recovery of NPA22 by absorbing water.

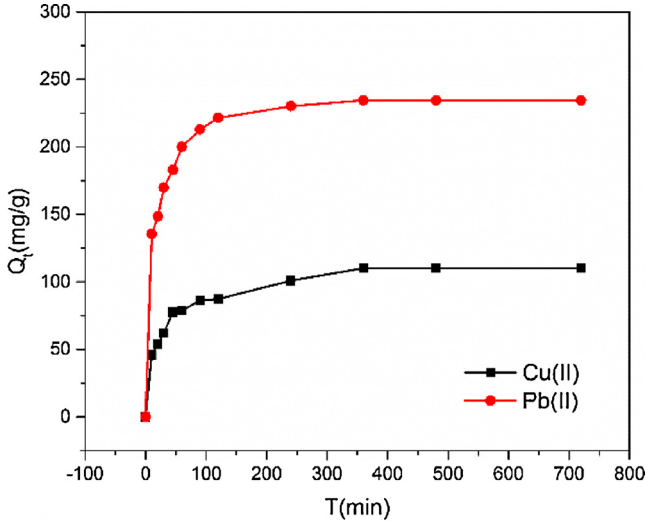

Fig. 5. Kinetic studies of Cu(II) and Pb(II) adsorption by NPA22.

of Cu(II) and Pb(II) ions by NPA22 was very fast and the adsorption reached equilibrium in 2 h, as showed in Fig. 5.

The fitting kinetic parameters from both models were summarized in Table 1. Both the values of the correlation coefficient (R^2) of the pseudo-first-order kinetic model for the adsorption of Cu(II) and Pb(II) were 0.999. These results suggested that the experimental data were described better by the pseudo- second -order kinetic model than the pseudo- first -order kinetic model. It also showed that the adsorption reaction of Cu(II) and Pb(II) was a chemical adsorption process (Aksu, 2002). It is well known that sorption kinetics is dependent on the functional groups of the adsorbents and adsorbent porosity. The satisfactory sorption velocities of NPA-2 for both Cu(II) and Pb(II) ions may be explained by the electrostatic attraction and cationic exchanges between the carboxyl, amine and the divalent Cu(II) and Pb(II) ions (Chen, Xue, & Li, 1995).

3.4. Adsorption isotherms

The adsorption isotherm parameters and graphics were displayed in Fig. 6 and Table 2, respectively. The higher correlation coefficient of the Langmuir model illustrated that the experimental data fit the

Table 1
Kinetic parameters for the adsorption of Cu(II) and Pb(II).

Metal ions	$Q_{e,e}$ (mg/g)	Pseudo-first-order equation			Pseudo-second-order equation		
		$Q_{e,c}$ (mg/g)	K_1	R^2	$Q_{e,c}$ (mg/g)	R^2	K_2
Cu(II)	138.40	82.41	0.0035	0.921	138.89	0.999	$3.98*10^{-4}$
Pb(II)	273.12	103.51	$3.11*10^{-3}$	0.844	270.27	0.999	$1.52*10^{-4}$

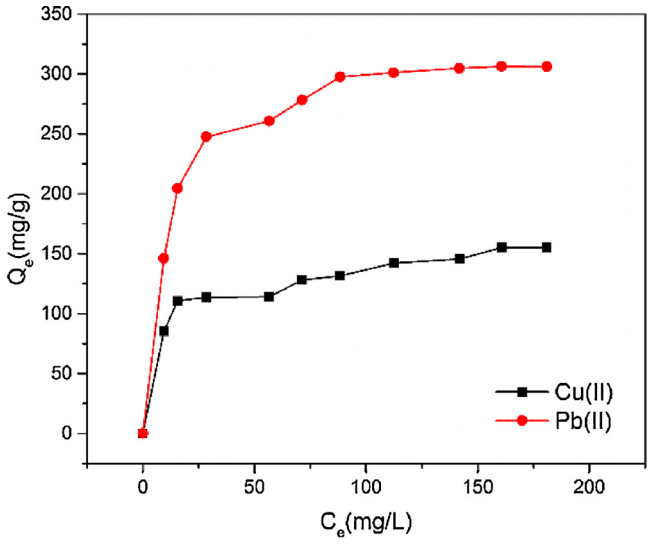

Fig. 6. Isotherms studies of Cu(II) and Pb(II) adsorption by NPA22.

Table 2
Isotherms parameters for the adsorption of Cu(II) and Pb(II).

	Langmuir Model				Freundlich Model		
	Qm (mg/g)	*b*	R_L	R^2	*n*	K_f	R^2
Cu(II)	175.44	0.033	0.13–0.60	0.999	4.00	40.93	0.961
Pb(II)	357.14	0.036	0.12–0.58	0.999	3.16	62.37	0.936

Langmuir model ($R^2 > 0.99$) better than the Freundlich model. The adsorption process was monolayer adsorption according to the assumptions of the Langmuir model (Liu, Ma, Xu, & Shao, 2010). This may be due to the electrostatic attraction between the carboxyl groups and the divalent metal ions, as well as the chelation between the amine groups and the metal ions. According to the Langmuir parameter, the theoretical adsorbed amounts of Cu(II) and Pb(II) were 175.44 mg/g and 357.13 mg/g, respectively. For Langmuir type adsorption process, the separation factor or equilibrium parameter (R_L) can be used to predict the advantage of adsorption, which is defined as Eq. (6) (Liu et al., 2010):

$$R_L = \frac{1}{1 + bC_0} \tag{6}$$

where C_o is the initial concentration and b is the Langmuir constant. When $0 < R_L < 1$, the adsorption process could be favorable. The calculated R_L values are listed in Table 2, which are all in the range of $0 < R_L < 1$, revealing that the Cu(II) and Pb(II) adsorption on NPA-2 are favorable (El-Reash, Otto, Kenawy, & Ouf, 2011).

3.5. Effect of solution pH

The pH is another major factor to influence the adsorption property. NPA22 was chosen as the experimental subject. When the pH was higher than 5.0, Cu(II) and Pb(II) ions in the solution were easily translated into $Cu(OH)_2$ and $Pb(OH)_2$ precipitation and could not be adopted. As shown in Fig. 7a, with the pH rising from 1.0 to 5.0, the absorption amount increased. The most suitable pH range was 2.0–5.0. It is noticeable that when the pH is lower than 2.0, little Cu(II) and Pb (II) ions can be adsorbed onto the NPA22. It was because that the amine groups could easily be protonated at lower pH, resulting in an electrostatic repulsive force to Cu(II) and Pb(II) ions and reducing adsorption ability.

3.6. Recycling performance

Recycling stability is also a significant factor for an adsorbent in the practical application. In general, desorption and regeneration of adsorbent are usually soaked in desorption agent, and then washed with aqueous solution. This method is not economic and requires a long time for desorption and purification. In this study, the absorbent of NPAs can be regenerated and reused simply by mechanically squeezing after adsorbing metal ions, due to the excellent wet strength and shape recovery property in water. As shown in Fig. 8, the water in the NPAs which contained metal ions is first squeezed by hand. EDTA solution is subsequently added to the NPAs until it recovers to the original shape. Then the NPAs are deposed for a period of time to complete the exchange of metal ion with EDTA. Above process is repeated several times to realize full desorption. Finally, the NPAs are purified with aqueous solution to remove EDTA using the same method. In comparison with the conventional methods, the squeezing method not only saves the dosage of EDTA, but also improves the efficiency of desorption and regeneration.

Fig. 7b shows the performance of NPA22 for Cu(II) and Pb(II) adsorption during 3 adsorption-desorption cycles. After three times of adsorption-desorption the adsorption capability remained relatively steady. The decrease of adsorption capacity in the second and third cycle might be because that some active sites of the absorbent combined with Cu(II) and Pb(II) in an irreversible way, thus reducing the density of Cu(II) and Pb(II) binding sites in the cycles. On the other hand, partial functional groups in NPA22 became to the protonated form during the regeneration process, which was unfavorable for Cu(II) and Pb(II) adsorption due to the decrease of electrostatic attraction between metal ions and NPA22.

Nowadays, nanocellulose-based materials are being used widely. Nanocellulose-based materials come from extensive sources and have shown decent adsorption performance. However, when nanocellulose-based materials are actually used for waste water treatment, the chemical modifications of these adsorbents were inevitable. Table 3 shows the theoretical maximum adsorption capacity for some nanocellulose-based materials used as heavy metal adsorbents reported in literature. Considering of adsorbent dosage, and so recycling process, the cost is somehow actually high. Compared to these adsorbents, NPAs showed better adsorption performance for removal of heavy metal ions from wastewater. In addition, the shape recovery of NPAs make the regeneration by EDTA leaching and purification more simple and economical. So we assume that NPAs are more competitive for practical use.

4. Conclusion

NPAs of NFC and PEI were prepared in a simple and green way via electrostatic combination. Based on the advantages of the highly porous structure, plenty of amine groups, high wet strength and excellent performance of water-activated shape recovery, NPAs were used as absorbent to remove heavy metal ions from aqueous solution. The maximum adsorption capacity of NPAs towards Cu(II) and Pb(II) reached 175.44 mg/g and 357.14 mg/g, respectively. The best fit for the experimental adsorption kinetic and isotherms data were pseudo-second-order and Langmuir model, respectively. In addition, EDTA solution could easily regenerate NPAs due to their shape recovery performance. After three adsorption/desorption cycles, the adsorption capacity of NPAs still maintained more than 90%.

Acknowledgments

The support of this work by the National Key Research and Development Program of China (2017YFD0601005), Natural Science Foundation of Jiangsu Province (BK20171450), National Natural Science Foundation of China (31370583, 31470599, 31770607) and

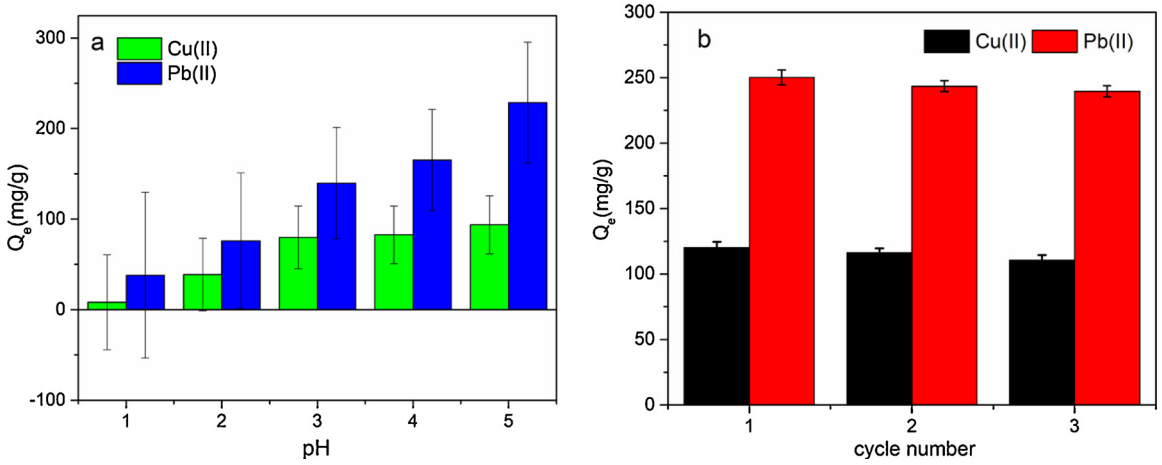

Fig. 7. (a) Effect of pH on Cu(II) and Pb(II) adsorption by NPA22; (b) The Cu(II) and Pb(II) equilibrium adsorption quantity by NPA22 in the adsorption-desorption experiment.

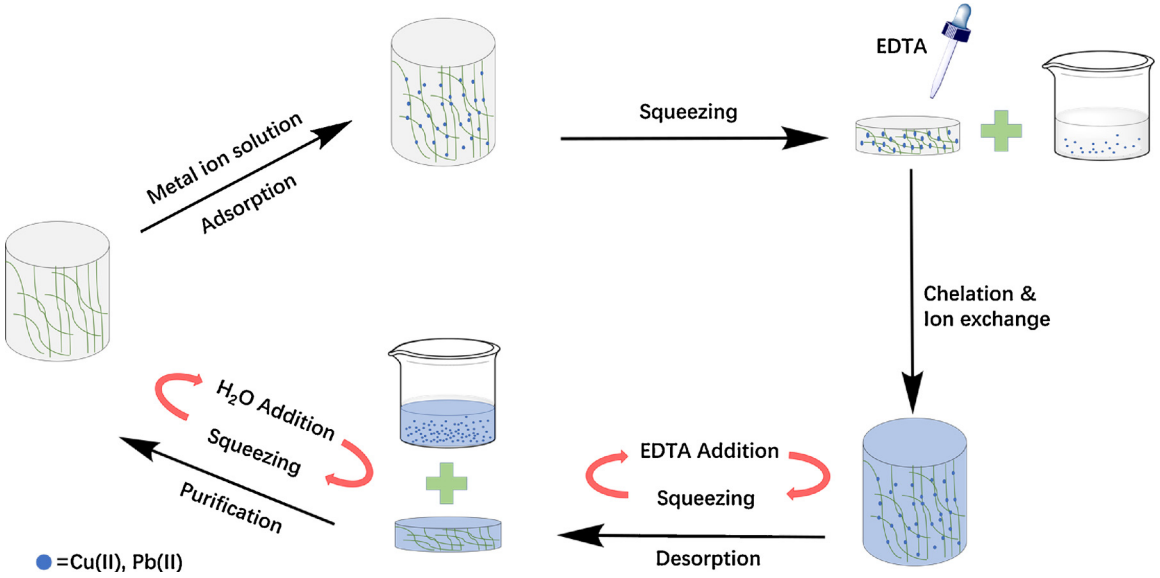

Fig. 8. The processing routes for desorption and regeneration of NPAs.

Table 3
The NPAs adsorption properties comparison of various nanocellulose-based adsorbents for the removal of Cu(II) and Pb(II).

Adsorbents	*Contaminant*	*pH*	Q_{max} (mg/g)	*Refs.*
NFC obtained through mechanical treatment	Pb^{2+}	5.5	10	Kardam, Raj, Srivastava, and Srivastava (2014).
NFC composite with CMC	Pb^{2+}	5	74.8	Chen et al. (2016)
NFC immobilized with black wattle tannin	Pb^{2+} Cu^{2+}	6	53.37 51.84	Xu, Wang, and Jin (2017)
CNC composite with bentonite	Pb^{2+}	5	91.2	Putro, Santoso, and Ismadji (2017)
NPA22	Pb^{2+} Cu^{2+}	5	357.14 175.44	This work

Priority Academic Program Development of Jiangsu Higher Education Institutions (PAPD) are gratefully acknowledged.

Appendix A. Supplementary data

Supplementary data associated with this article can be found, in the online version, at https://doi.org/10.1016/j.carbpol.2018.05.015.

References

Adebajo, M. O., Frost, R. L., & Kloprogge, J. T. (2003). Porous materials for oil spill cleanup: A review of synthesis and absorbing properties. *Journal of Porous Materials, 10*, 159–170.
Aksu, Z. (2002). Determination of the equilibrium, kinetic and thermodynamic parameters of the batch biosorption of nickel(II) ions onto Chlorella vulgaris. *Process Biochemistry, 38*, 89–92.
Barrera-Díaz, C. E., Lugo-Lugo, V., & Bilyeu, B. (2012). A review of chemical: Electrochemical and biological methods for aqueous Cr (VI) reduction. *Journal of Hazardous Materials, 223*, 1–12.
Benhamou, K., Dufresne, A., Magnin, A., & Mortha, G. (2014). Control of size and viscoelastic properties of nanofibrillated cellulose from palm tree by varying the TEMPO-mediated oxidation time. *Carbohydrate Polymers, 99*, 74–83.
Carta, D., Casula, M. F., & Corrias, A. (2009). Structural and magnetic characterization of Co and Ni silicate hydroxides in bulk and in nanostructures within silica aerogels. *Chemistry of Materials, 21*, 945–953.
Chen, S., Xue, M., & Li, F. (1995). Thermal and pH-response of dimethylaminoethyl methylacrylate and its polymer. *Acta Polymerica Sinica* 373–373.
Chen, W., Lickfield, G. C., & Yang, C. Q. (2004). Molecular modeling of cellulose in amorphous state. Part I: Model building and plastic deformation study. *Polymer, 45*, 1063–1071.
Chen, W., Li, Q., & Wang, Y. (2014). Comparative study of aerogels obtained from differently prepared nanocellulose fibers. *ChemSusChem, 7*, 154–161.
Chen, B., Zheng, Q., Zhu, J., Li, J., Cai, Z., Chen, L., et al. (2016). Mechanically strong fully biobased anisotropic cellulose aerogels. *RSC Advances, 6*, 96518–96526.

Chen, W. S. (2011). Ultralight and highly flexible aerogels with long cellulose I nanofibers. *Soft Matter, 7*, 10360–10368.
Cong, H. P. (2012). Macroscopic multifunctional graphene-based hydrogels and aerogels by a metal ion induced self-assembly process. *ACS Nano, 6*, 2693–2703.
Dong, H. (2013). Hydrogel, aerogel and film of cellulose nanofibrils functionalized with silver nanoparticles. *Carbohydrate Polymers, 95*, 760–767.
El-Reash, Y. G. A., Otto, M., Kenawy, I. M., & Ouf, A. M. (2011). Adsorption of Cr (VI) and As (V) ions by modified magnetic chitosan chelating resin. *International Journal of Biological Macromolecules, 49*, 513–522.
Fukuzumi, H., Saito, T., & Isogai, A. (2013). Influence of TEMPO-oxidized cellulose nanofibril length on film properties. *Carbohydrate Polymers, 93*, 172–177.
Ge, D., Yang, L., & Li, Y. (2009). Hydrophobic and thermal insulation properties of silica aerogel/epoxy composite. *Journal of Non-Crystalline Solids, 355*, 2610–2615.
Hüsing, N., & Schubert, U. (1998). Aerogele–luftige materialien: Chemie, struktur und eigenschaften. *Angewandte Chemie, 110*, 22–47.
Heath, L., & Thielemans, W. (2010). Cellulose nanowhisker aerogels. *Green Chemistry, 12*, 1448–1453.
Hong, & Joo, H. (2009). Preparation of an anion-exchange membrane by the amination of chlorinated polypropylene and polyethyleneimine at a low temperature and its ion-exchange property. *Journal of Applied Polymer Science, 112*, 830–835.
Isogai, A. (2013). Wood nanocelluloses: Fundamentals and applications as new bio-based nanomaterials. *Journal of Wood Science, 59*, 449–459.
Kardam, A., Raj, K. R., Srivastava, S., & Srivastava, M. M. (2014). Nanocellulose fibers for biosorption of cadmium, nickel, and lead ions from aqueous solution. *Clean Technologies and Environmental Policy, 16*, 385–393.
Khodadadi, M., Malekpour, A., & Ansaritabar, M. (2017). Removal of Pb (II) and Cu (II) from aqueous solutions by NaA zeolite coated magnetic nanoparticles and optimization of method using experimental design. *Microporous and Mesoporous Materials, 248*, 256–265.
Liang, H. W., Guan, Q. F., Chen, L. F., Zhu, Z., Zhang, W. J., & Yu, S. H. (2012). Macroscopic-Scale template synthesis of robust carbonaceous nanofiber hydrogels and aerogels and their applications. *Angewandte Chemie International Edition, 51*, 5101–5105.
Liu, J., Ma, Y., Xu, T., & Shao, G. (2010). Preparation of zwitterionic hybrid polymer and its application for the removal of heavy metal ions from water. *Journal of Hazardous Materials, 178*, 1021–1029.
Lu, P., Hsieh, & You, L. (2012). Preparation and characterization of cellulose nanocrystals from rice straw. *Carbohydrate Polymers, 8*, 7564–7573.
Mishra, P. C., & Patel, R. K. (2009). Removal of lead and zinc ions from water by low cost adsorbents. *Journal of Hazardous Materials, 168*, 319–325.
Nair, S. S., Zhu, J. Y., & Deng, Y. (2014). Hydrogels prepared from cross-linked nanofibrillated cellulose. *ACS Sustainable Chemistry & Engineering, 2*, 772–780.
O'Connell, D. W., Birkinshaw, C., & O'Dwyer, T. F. (2008). Heavy metal adsorbents prepared from the modification of cellulose: A review. *Bioresource Technology, 99*, 6709–6724.
Owlad, M., Aroua, M. K., Daud, W. A. W., & Baroutian, S. (2009). Removal of hexavalent chromium-contaminated water and wastewater: A review. *Water, Air, and Soil Pollution, 200*, 59–77.
Putro, J. N., Santoso, S. P., & Ismadji, S. (2017). Investigation of heavy metal adsorption in binary system by nanocrystalline cellulose–bentonite nanocomposite: Improvement on extended Langmuir isotherm model. *Microporous and Mesoporous Materials, 246*, 166–177.
Sakurada, I., Nukushina, Y., & Ito, T. (1962). Experimental determination of the elastic modulus of crystalline regions in oriented polymers. *Journal of Polymer Science Part A: Polymer Chemistry, 57*, 651–660.
Salama, A., Shukry, N., & El-Sakhawy, M. (2015). Carboxymethyl cellulose-g-poly (2-(dimethylamino) ethyl methacrylate) hydrogel as adsorbent for dye removal. *International Journal of Biological Macromolecules, 73*, 72–75.
Sui, Z. Y., Cui, Y., Zhu, J. H., & Han, B. H. (2013). Preparation of three-dimensional graphene oxide–polyethylenimine porous materials as dye and gas adsorbents. *ACS Applied Materials & Interfaces, 5*, 9172–9179.
Wang, J., & Chen, C. (2006). Biosorption of heavy metals by Saccharomyces cerevisiae: A review. *Biotechnology Advances, 24*, 427–451.
Wang, Y. Y., Tian, M., & Xu, H. X. (2014). Influence of moisture on mechanical properties of cellulose insulation paper. *International Journal of Modern Physics B, 28*, 1450051.
Xu, Q., Wang, Y., & Jin, L. (2017). Adsorption of Cu (II), Pb (II) and Cr (VI) from aqueous solutions using black wattle tannin-immobilized nanocellulose. *Journal of Hazardous Materials, 339*, 91–99.
Zander, & Nicole, E. (2014). Metal cation cross-linked nanocellulose hydrogels as tissue engineering substrates. *ACS Applied Materials & Interfaces, 6*, 18502–18510.
Zhang, W., Zhang, Y., & Lu, C. H. (2012). Aerogels from crosslinked cellulose nano/microfibrils and their fast shape recovery property in water. *Journal of Materials Chemistry, 22*, 11642–11650.
Zhang, N., Zang, G. L., & Shi, C. (2016). A novel adsorbent TEMPO-mediated oxidized cellulose nanofibrils modified with PEI: Preparation, characterization, and application for Cu (II) removal. *Journal of Hazardous Materials, 316*, 11–18.
Zheng, Q., Cai, Z., & Gong, S. (2014). Green synthesis of polyvinyl alcohol (PVA)–cellulose nanofibril (CNF) hybrid aerogels and their use as superabsorbents. *Journal of Materials Chemistry A, 2*, 3110–3118.
Zimmermann, T., Bordeanu, N., & Strub, E. (2010). Properties of nanofibrillated cellulose from different raw materials and its reinforcement potential. *Carbohydrate Polymers, 79*, 1086–1093.